Crystal structures of pertussis toxin with NAD$^+$ and analogs provide structural insights into the mechanism of its cytosolic ADP-ribosylation activity

Received for publication, January 20, 2022, and in revised form, March 17, 2022 Published, Papers in Press, April 1, 2022,
https://doi.org/10.1016/j.jbc.2022.101892

Moona Sakari[1], Mai T. Tran[2], Jamie Rossjohn[2,3], Arto T. Pulliainen[1,*], Travis Beddoe[4,*], and Dene R. Littler[2,*]

From the [1]Institute of Biomedicine, Research Unit for Infection and Immunity, University of Turku, Turku, Finland; [2]Infection and Immunity Program & Department of Biochemistry and Molecular Biology, Biomedicine Discovery Institute, Monash University, Clayton, Victoria, Australia; [3]Institute of Infection and Immunity, School of Medicine, Cardiff University, Heath Park, Cardiff, Wales, UK; [4]Department of Animal, Plant and Soil Science and Centre for AgriBioscience, La Trobe University, Bundoora, Victoria, Australia

Edited by Ursula Jakob

***Bordetella pertussis* is the causative agent of whooping cough, a highly contagious respiratory disease. Pertussis toxin (PT), a major virulence factor secreted by *B. pertussis*, is an AB5-type protein complex topologically related to cholera toxin. The PT protein complex is internalized by host cells and follows a retrograde trafficking route to the endoplasmic reticulum, where it subsequently dissociates. The released enzymatic S1 subunit is then translocated from the endoplasmic reticulum into the cytosol and subsequently ADP-ribosylates the inhibitory alpha-subunits (Gαi) of heterotrimeric G proteins, thus promoting dysregulation of G protein–coupled receptor signaling. However, the mechanistic details of the ADP-ribosylation activity of PT are not well understood. Here, we describe crystal structures of the S1 subunit in complex with nicotinamide adenine dinucleotide (NAD+), with NAD+ hydrolysis products ADP-ribose and nicotinamide, with NAD+ analog PJ34, and with a novel NAD+ analog formed upon S1 subunit crystallization with 3-amino benzamide and NAD+, which we name benzamide amino adenine dinucleotide. These crystal structures provide unprecedented insights into pre- and post-NAD+ hydrolysis steps of the ADP-ribosyltransferase activity of PT. We propose that these data may aid in rational drug design approaches and further development of PT-specific small-molecule inhibitors.**

The highly contagious bacteria *Bordetella pertussis* infects millions of people each year. *B. pertussis* infection is particularly dangerous for infants and young children where it may progress into whooping cough, a life-threatening respiratory disease (1). Thankfully the historical burden of whooping cough has been dramatically curtailed by the widespread deployment of successful vaccination strategies now covering majority of the global population (1). While pertussis-linked deaths continue to claim around 200,000 infants per year, the vast majority of such cases originate in areas of the world where immunization coverage is inadequate (2). Vaccinated populations display marked morbidity reduction, but *B. pertussis* continues to circulate, providing a bacterial reservoir that can expand to cause endemic outbreaks. Moreover, developed nations have experienced rises in the number of pertussis cases reported; this has been attributed to waning adult immunity (3), bacterial divergence from vaccine strains (4) and incomplete vaccine coverage (5). Indeed, *B. pertussis* infection has become one of the most prevalent vaccine-preventable diseases.

B. pertussis expresses an array of virulence factors that promote bacterial adhesion and invasion but also prevent the onset of a protective immune responses (1). Subversion of the host's innate and adaptive immune systems is achieved through secretion of pertussis toxin (PT), a multifaceted protein complex that targets resident airway macrophages (6) and inhibits neutrophil recruitment at sites of infection to delay antibody-mediated clearance (7). In addition, PT-mediated disruption of tight junctions between airway epithelial cells, linked to the development of pulmonary edema, and PT-mediated blockage of anti-inflammatory cell signaling, linked to the prolonged duration of respiratory inflammation, have been proposed (8). PT is central to the pathogenesis of whooping cough (9, 10) as *Bordetella* strains unable to express it fail to elicit the severe coughing fits characteristic of the disease in rat models (11, 12). The resurgence of pertussis infection in vaccinated populations has also been associated with the spread of more virulent bacterial strains with increased PT expression (13). Inactivated forms of PT are thus considered an essential component of acellular and cellular vaccines (14), and the protective immune response following vaccination or an individual's recovery from infection results in part from the induced reservoir of anti-PT antibodies (15). Directly targeting bacterial virulence factors is a novel therapeutic strategy (16). Recently, PT-neutralizing monoclonal antibodies (17) and small-molecular-weight compounds (18, 19) have been identified, possibly leading to new therapeutic options to prevent and treat the whooping cough.

PT is a complex bacterial exotoxin as it is secreted as an inactive 105-kDa heterohexamer composed of six subunits. The

* For correspondence: Dene R. Littler, dene.littler@monash.edu; Arto T. Pulliainen, arto.pulliainen@utu.fi; Travis Beddoe, t.beddoe@latrobe.edu.au.

structure of this secreted form of PT is known, in it the S1 subunit contains an enzymatic ADP-ribosyltransferase (ART) domain that sits atop a pseudo-pentameric ring–like arrangement of structurally similar glycan-binding subunits S2:S5:S4:S3:S4 (20, 21). This stoichiometry is a more complex variant of the AB_5-type bacterial exotoxins (20), a family that includes the orthologous typhoid (22) and pertussis-like toxins (23) and the distantly related cholera and heat-labile toxins (24). The glycan-binding subunits of PT mediate host cell recognition through affinity for sialylated sugars attached to proteins at the host cell plasma membrane (21). The glycan binding results in PT internalization and retrograde trafficking into the endoplasmic reticulum (ER) (25). In the ER, binding of ATP to PT destabilizes the interaction between the S1 subunit and the B5 pentamer, leading into dissociation of the S1 subunit (26, 27). The folding properties of the thermally unstable S1 subunit favor its transport from the ER into the cytosol *via* the ER-associated degradation pathway (28, 29). It has been reported that cyclophilins, peptidyl prolyl cis/trans isomerases, are involved in this ER-to-cytosol transport (19, 30). In the cytosol, the S1 toxin subunit catalyzes the transfer of the ADP-ribose moiety from nicotinamide adenine dinucleotide (NAD+) onto a specific C-terminal cysteine of the inhibitory α-subunits ($G\alpha_i$) of heterotrimeric G proteins (31). This modification provides a steric barrier that prevents $G\alpha_i$ proteins interfacing with their cognate G protein–coupled receptors, rendering them unable to function, disrupting $G\alpha_i$-mediated signaling, and resulting in the toxin's pathochemistry.

While the initial steps of host glycan recognition are well understood for PT (20, 21), the molecular mechanisms by which the S1 domain becomes enzymatically active and catalyzes the ART reaction have remained elusive. In the AB_5 holotoxin, the C-terminus (residues 180–235) of the S1 subunit prevents its enzymatic ART activity (20, 21). The C-terminus is held within the NAD+-binding site by an intramolecular disulfide bond (20, 21). Enzymatic activation requires the reducing environment of the cytoplasm to reduce this disulfide bond and release the C-terminus' inhibitory effect. It has also been proposed that the C-terminus is proteolytically cleaved inside the host cell, but this does not seem to drastically affect the catalytic activity of S1 (32). Truncated forms of the S1 domain lacking the inhibitory C-terminus, such as the one used in this study, are constitutively active enzymes *in vitro* (18). To help guide a better understanding of the ART activity of PT, herein we present the first crystal structures of the S1 catalytic domain in complex with NAD^+ and a number of different NAD+ analogs. We detail the structural changes that occur upon binding, providing structural details of the protein's catalytic mechanism including snapshots of its pre- and post-NAD+ hydrolysis states that may aid inhibitor design.

Results

Structures of pre- and post-NAD+ hydrolysis states of PT S1 subunit

In order to obtain a structure of S1 in complex with NAD^+, we utilized enzymatically impaired versions as the S1 will still display NAD+ hydrolysis activity in the absence of its Gαi protein substrate (18). We trialed different mutations of the catalytically critical Glu-129 to obtain crystals of the S1 subunit in a NAD^+-bound state but also found that the wildtype protein remained catalytically nonpermissive in the presence of 200 mM potassium iodide. We were able to obtain high-resolution NAD+-bound crystal structures of the E129D S1 mutant and in the presence of iodide ions also of the wildtype S1, referred to as $S1_{E129D}$ and $S1_{NAD}$, respectively. For further structural comparison, we obtained a crystal structure of the active site loop C41S S1 mutant with nominal catalytic activity in complex with the products of the S1 NAD+ hydrolysis activity, ADP-ribose, and nicotinamide (referred to as $S1_{ADPR/NA}$). Initial phases for these structures were obtained using the PT holotoxin's S1 subunit (PDB: 1BCP referred to as $S1_{APO}$) (27) as a molecular replacement model followed by rounds of manual building and refinement (see Table S1 and Experimental procedures for details). $S1_{NAD}$ crystallized in space group P1 with four molecules within the asymmetric unit. The Cα-backbone traces of all four protomers are nearly identical except across residues 112 to 129, which adopts multiple alternate conformations (helix h5 of the holotoxin, see Fig. 1 for numbering). In some protomers, the density for these residues does not permit them to be modeled. In the pre-NAD+ hydrolysis states ($S1_{NAD}$ or $S1_{E129D}$), clear electron density allowed unambiguous placement for all atoms of the bound NAD^+ (Fig. S1*A*), likewise for ADP-ribose and nicotinamide within the electron density of the post-NAD+ hydrolysis $S1_{ADPR/NA}$ crystals (Figs. 1 and S1*B*).

The S1 subunit mimics a partially folded endogenous protein as a mechanism by which to exit the ER by hijacking the ER-associated degradation pathway; it then escapes degradation within the cytosol where it is reduced and activated (29). Indeed, the transition to the active B5-free S1 subunit results in significant structural changes with conformational heterogeneity. In each of our structures, the four molecules of PT within the asymmetric unit can display different conformations within the flexible loop immediately prior to the catalytic Glu-129 (Fig. S2, *A* and *B*). This flexible loop is highly enriched for small amino acids (^{112}GDNAGRILAGALATYQ^{127}) that undergo large shifts in Ramachandran space during these transitions. The structural variation in this region of the protein appears inherent, and the different forms of the loop are observed irrespective of the nucleotide bound (Fig. S2, *C*–*E*). We note that the equivalent plastic region of the protein is thought to mediate Gαi protein recognition in related toxins (33).

S1 subunit structural changes occurring upon NAD+ binding

We compared the $S1_{NAD}$ structure with that of the catalytically inhibited intramolecular disulfide-bonded $S1_{APO}$ form (27). In $S1_{APO}$, the inhibitory C-terminus threads between h2 and h5 and then forms a small β-sheet overlaying the pseudopentamer pore before delving into it (Fig. 1). This inhibitory structure securely connects the cargo S1 subunit with its glycan-binding B5 carrier subunits. However, in doing so, the NAD+-binding site is completely occluded by the inhibitory C

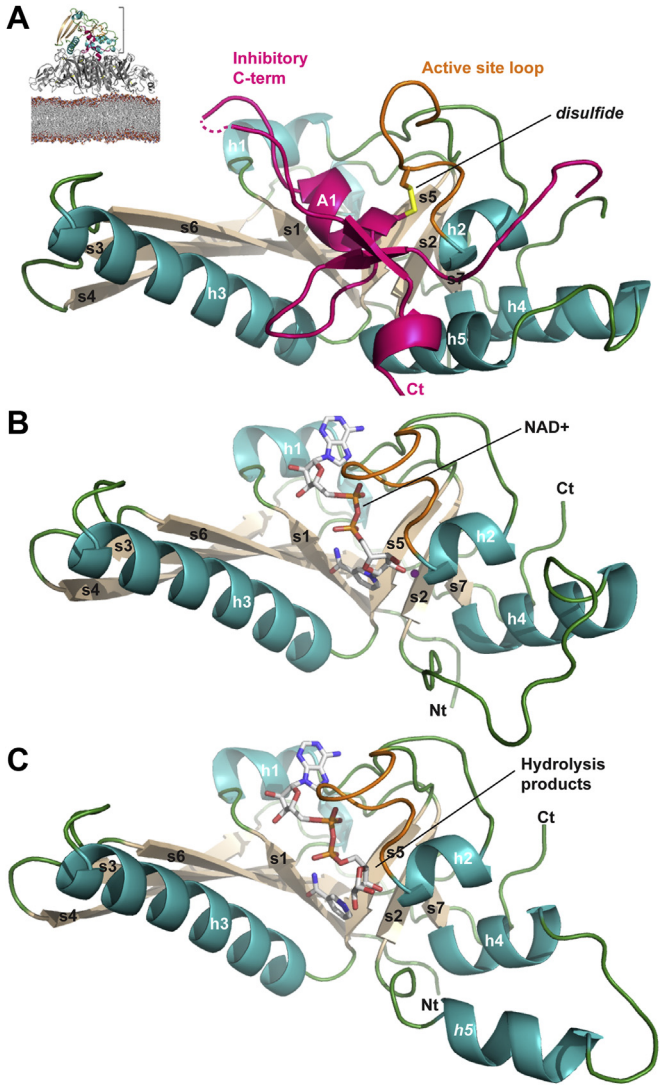

Figure 1. Overview of the apo and NAD+-bound as well as ADP-ribose–and nicotinamide-bound PT. *A–C*, cartoon representation of the structure of the catalytic segment of the PT S1 subunit in (*A*) the AB_5 holotoxin ($S1_{APO}$, PDB 1PRT) and (*B*) the C-terminal truncated NAD-bound state ($S1_{NAD}$, this study) and (*C*) hydrolyzed NAD+ state ($S1_{ADPR/NA}$ this study). Secondary structural elements are labeled with α-helices colored *teal*; β-strands *tan*; the inhibitory C-terminus *pink*, and the active site loop *orange*. NAD^+ and the disulfide residues are depicted in ball-and-stick representation. The *insert* indicates the position of the S1 subunit within the PT hetero-hexameric complex (20) with the host cell surface glycan-binding subunits colored *gray*. NAD+, nicotinamide adenine dinucleotide; PT, pertussis toxin.

terminus, which is pinned to one wall of the U-shaped cleft by the disulfide between Cys-41 and Cys-201 (*pink* in Fig. 1*A*). At ∼12 Å, this inhibitory helix is significantly wider than the NAD+ substrate (6-8 Å thick). Significant structural rearrangements occur following the binding of NAD+ to S1 (Figs. 1*B* and 2*A*). Following the loss of the C-terminal residues, the NAD+-binding cleft walls are able to contract inward. The h2 helix and its connecting loop regions Gly-27 and Ala-49 act as pivot points for a rigid-body rotation that serves to move the C-terminus of h2 approximately 3 Å closer until it contacts the N-ribose of NAD^+ (Fig. 2*A*). On the other side of the nucleotide, the h3 helix rotates ∼5° inward about its N-terminus, facilitating contact with the nicotinamide. The residues within the active-site loop (^{41}CQVGSS^{46}) also undergo significant refolding. This loop is held aloft by Arg-204 within the h6 helix but refolds to serve as an enclosing clamp over the nucleotide-binding site in $S1_{NAD}$. The thiol group of Cys-41 drops down to interleave between the two phosphates, while Gln-42 undergoes one of the largest activation-induced movements, with its amide swiveling 15.4 Å to overlay the A-ribose and A-phosphate sealing the site.

The nature of the nucleotide binding-site means that NAD^+ is effectively sandwiched across its length between residues from each of the two β-cores. The dissociation of the h6 helix has a more substantial effect on the one end of the binding cleft than the other. Only minor rotamer changes for residues are required to convert into the ADP-interacting section of the cleft, whereas more significant reconstruction occurs at the opposite nicotinamide end. Within the $S1_{APO}$, Met-202 inserts into a hydrophobic pocket between residues of a conserved ^{52}STS^{54}-motif; this is cleared upon reduction allowing the nicotinic ring of NAD^+ to replace it and its amide group simultaneously forming a β-sheet–like interaction with Tyr-10. This hydrophobic pocket shrinks upon activation through the inward rotation of the h3 helix by ∼5°; a movement that allows the hydroxyl of Tyr-63 to hydrogen bond with the N-phosphate.

At the nicotinamide end, the microenvironment around the catalytic Glu-129 also displays significant remodeling. Within the $S1_{APO}$, the charged carboxyl group of Glu-129 parks within a buried yet polar environment, hydrogen bonds being formed to His-35, Ser-52, and Gln-127. Upon NAD+ binding, this microenvironment becomes more hydrophobic. The rigid-body migration of h2 toward the nucleotide allows the side chain of Leu-34 to encroach upon Glu-129; meanwhile, His-35 moves behind Leu-131 and Gln-127 exits the cleft entirely. These changes leave the catalytic glutamate within a shell of hydrophobic residues, maturing the active site into a form more closely resembling that of other ART enzymes (34). Burying a charged glutamate within a hydrophobic environment alters the local dielectric and can serve to raise the pK_a of catalytic residues by several units (35).

S1 subunit structural changes occurring upon NAD+ hydrolysis

The $S1_{ADPR/NA}$ structure in complex with nicotinamide and ADP-ribose was obtained when C41S S1 mutant was incubated with NAD+ prior to crystallization and diffraction data collection (Fig. 1*C*). Hydrolysis of the glycosidic bond of NAD+ is an alternate reaction that occurs when a water molecule acts as an attacking nucleophile in place of a protein substrate amino acid. While activation and NAD+ binding to S1 result in considerable structural changes, hydrolysis of nicotinamide is more nuanced with a small opening of h3 (Fig. 2*B*). Following cleavage of the scissile bond, the reaction products remain largely in place except for one important exception: the rotation by ∼130° of the newly liberated N-ribose about the P_N-O_5 bond (Fig. 3, *A* and *B*). This places ADP-ribose in a more extended conformation, with the N-ribose's hydroxyls directed toward helix 2. In this state, the newly added 1′-hydroxyl lies directly under the C-terminus of

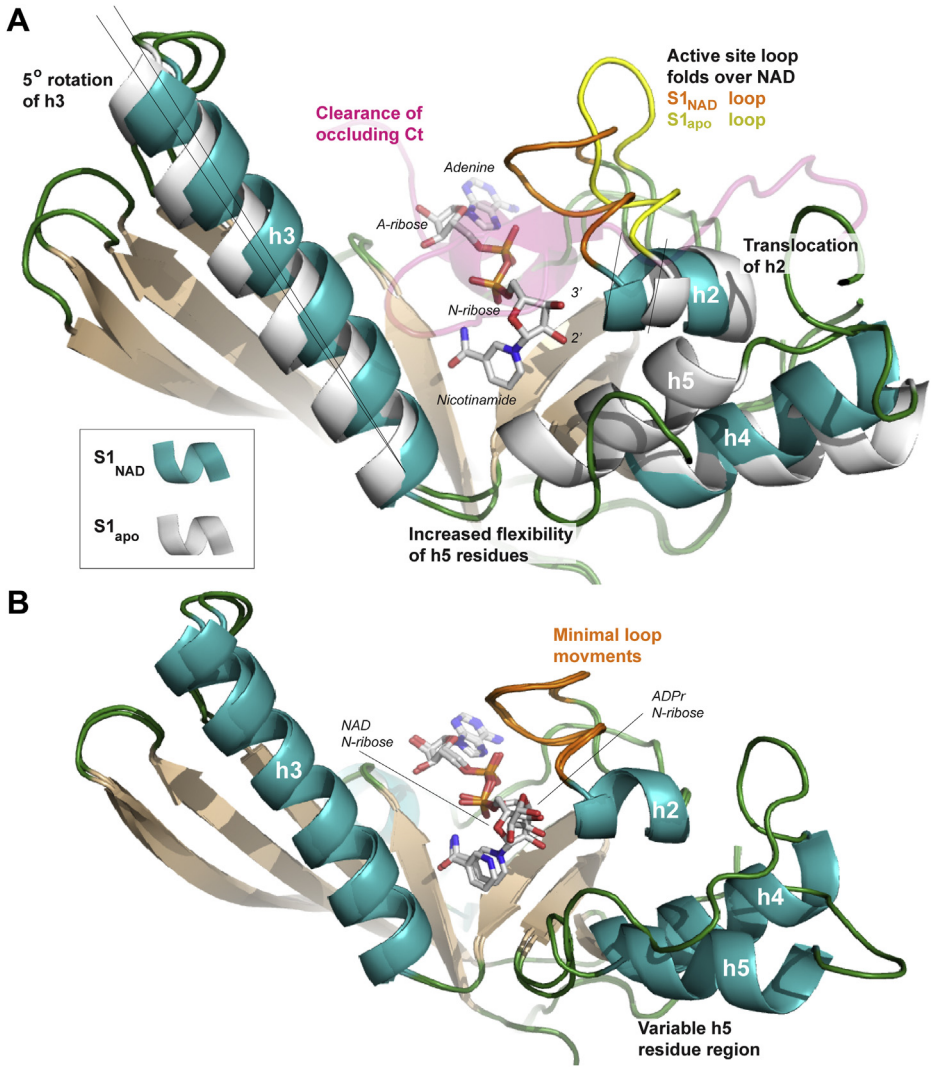

Figure 2. Comparison of the apo and NAD+-bound as well as ADP-ribose– and nicotinamide-bound PT S1. *A*, cartoon overlay of the catalytic domain within the PT $S1_{NAD}$ (*teal* helices) and PT $S1_{APO}$ (transparent *gray* helices). The major structural changes discussed in text are highlighted. *B*, an equivalent overlay of PT $S1_{NAD}$ and PT $S1_{ADPR/NA}$ depicting the more nuanced differences observed between pre- and post-NAD+ hydrolysis states. NAD+, nicotinamide adenine dinucleotide; PT, pertussis toxin.

helix 2, a position that may allow the helix's polar dipole to stabilize an oxocarbenium intermediate. After this N-ribose rotation, Glu-129 forms a direct hydrogen bond with the 3′-hydroxyl, while the 2′-hydroxyl is relegated to a bridged water-mediated contact. The rotation of the ribose is accommodated by the S1 through a ∼0.8-Å shift of the h2 helix away from the nucleotide. Unlike the 3-Å inward movement of h2 that occurs during the transition from $S1_{APO}$ to $S1_{NAD}$, this smaller h2 movement in $S1_{ADPR/NA}$ occurs with minimal changes within the active loop. The ADP section of the nucleotide as well as its binding site within the active PT remains entirely static throughout this process.

Structural requirements for the ADP-ribosylation reaction in S1

To assess which residues of S1 are catalytically essential for its ART activity, we made and purified S1 mutants with single-amino-acid alterations. Activity was assessed by monitoring each mutant's ability to transfer biotin as part of a modified NAD+ analog onto purified human G protein substrate (*Hs*Gαi3, Fig. 3*D*), an assay we have used previously (23). This assay (Fig. 3*D*) recapitulated the results of others (36) in that E129D mutant is catalytically inactive while C41S mutant displays activity indistinguishable from wildtype S1 (37). We observed two tyrosines (Y59 and Y63) within helix 3 enclosing upon the nicotinamide group in the substrate-bound state (Fig. 3*A*); we sought to assess whether enzymatic activity might depend on these new conformations by converting each residue to alanine (Fig. 3*D*). Loss of either tyrosine drastically reduced activity of the S1 subunit in the *in vitro* assays (Fig. 3*D*). No detectable activity was observed for the Y59A mutant, whereas the Y63A mutant retained activity ∼5% of that of wildtype.

We further sought to identify regions of the S1 that might interact with the Gαi protein substrate. Bulky additions were thus inserted in order to disrupt potential protein interfaces on

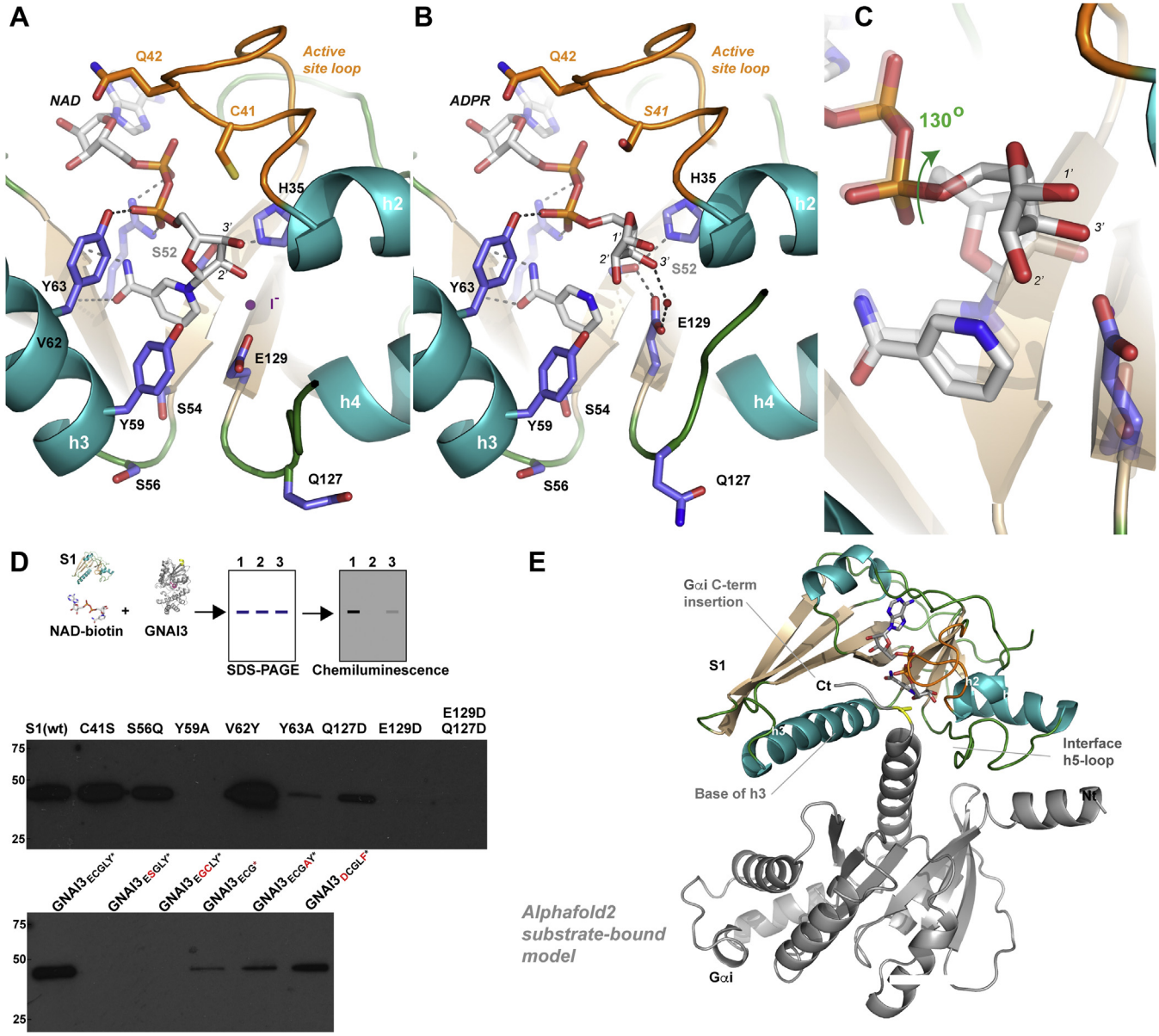

Figure 3. Catalytic residues of PT S1 surrounding the scissile nicotinamide bond in pre- and post-NAD+ hydrolysis states. *A* and *B*, ball-and-stick representation of the residues within the S1 active site (A) before ($S1_{NAD}$) and (B) after hydrolysis of the nicotinamide bond of NAD+ ($S1_{ADPR/NA}$). For clarity, the carbon atoms of NAD+, ADP-ribose, and nicotinamide are colored *gray*, while those of depicted protein residues are colored *navy blue*. Residues are labeled with *bold* font, and the inactivating iodide ion in (a) is shown as a *purple* sphere. *C*, for greater clarity, an overlay of the nicotinamide ribose movements are shown in which the NAD+-bound state is partially transparent. *D*, to explore which residues within the toxin and G proteins were important for ADP-ribosyltransferase activity, an *in vitro* assay using biotinylated substrate was established. Residues within, and near, the PT S1 domain's active site were first mutated (*top panel*), followed by mutations in the human G protein substrate (*bottom panel*). *E*, examples of plausible Alphafold2-based models of the PT:$GNAI3_{mini}$ interaction. The Gαi C-terminal domain is displayed in *gray*, with the modified C-terminal cysteine highlighted in *yellow*. NAD+, nicotinamide adenine dinucleotide; PT, pertussis toxin.

the external face of helix 3 (V62Y) and the C-terminus of S2 (S54Q). Our measured enzymatic activity was unaffected in the presence of either mutation (Fig. 3*D*), indicating that these may not be sites of protein interaction with the G protein. In ART enzymes, a glutamine (Q127 in PT) two residues prior the catalytically essential glutamate is often involved in catalysis (38). In our structures, Q127 is situated at the base of the flexible loop that forms h5 within the holotoxin; despite being near the catalytic residue E129, it was generally observed facing away from the NAD^+-binding site and toward solvent. We next sought to test what the effect of a Q127D mutant would be on ADP-ribosylation activity and observed a ∼50% reduction in *Hs*Gαi3 modification. This indicative reduced activity and/or substrate binding was consistent with a potential role for Q127 in facilitating catalysis, albeit one that is nonessential.

Structural requirements for the ADP-ribosylation reaction in Gαi

The toxin's S1 subunit transfers ADP-ribose from NAD+ onto Cys-351 within human Gαi subunits, four residues from their C-termini. We next altered the C-terminal residues within the recombinant human Gαi3 protein from that of the

wildtype sequence ^{350}ECGLY*^{354}. Four mutations within this sequence were made, expressed and purified, and tested for their ability to act as substrates in our *in vito* ADP-ribosylation assays (Fig. 3*D*). As expected, enzymatic activity of S1 required the presence of its target residue as *Hs*Gαi3 (C351S) mutants were entirely resistant to modification (Fig. 3*D*). Swapping C351 with the following residue, G352, also obliterated activity (*bottom panel* Fig. 3*D*), indicating that the cysteine's position is vitally important. Other mutants had less of an effect on substrate suitability. Truncation of the C-terminal residue Y354 reduced activity ∼5-fold based on densitometry but did not eliminate it. Loss of the β-branched residue within the mutant *Hs*Gαi3 (L353A) had minimal effect upon its suitability to act as a substrate (*bottom panel* Fig. 3*D*); conversion to an *Hs*Gαi2-like sequence DCGLF*^{354} gave signal equivalent to wildtype protein.

Alphafold2 (39) modeling of $S1_{NAD}$ complexed with G protein substrate sequences suggests a number of potential docking modes for the C-terminal helix of Gαi proteins (*e.g.* Figs. 3*E* and S3*A*). The cysteine residue modified by PT within Gαis are four residues from the G protein's termini and are the C-capping residue of α5, part of a helix that rotates depending upon the bound nucleotide present and whose C-terminal residues become ordered when GPCR-engaged (40) (Fig. S3, *B* and *C*). The structural rotation of the Gαi-α5 helix complicates potential S1-binding interfaces as the external facing residues can thus vary. Alphafold2 preferentially modeled S1 engaged with Gαi using a helical structure more akin to the GPCR-bound form (Fig. S3*D*). In such computational models, the conserved hydrophobic residues within the sequence ^{344}IKNNLKE**C**GLF^{354} interacted directly with S1 residues Y59 and Y63 which were generally in NAD+-bound positions.

Structure of S1 subunit with a novel NAD+ analog

We next explored the S1 binding mode of broad-specificity mimetics of nicotinamide. 3-Amino benzamide (3AB) is one such compound and can be described as a near-minimal nicotinamide mimic, which inhibited S1-catalyzed Gαi ADP-ribosylation activity at millimolar concentrations (Fig. 4*A*). We were unable to obtain a stable co-complex between 3AB and S1, potentially because the inherent flexibility of S1 (Fig. S2*B*) may result in constant assembly and disassembly of its nicotinamide-binding site. However, we also attempted to co-crystallize S1 together with 3AB and NAD+. The high 1.0-Å resolution of this structure (referred to as $S1_{BaAD}$) was highly advantageous as 3AB was seen to displace nicotinamide-binding location in S1 (Fig. 4*B*). Furthermore, we witnessed a covalent bond between the anomeric carbon of N-ribose and the aniline nitrogen of 3AB, indicating formation of a novel NAD+ analog at the catalytic center of S1. We term this novel NAD+ analog as benzamide amino adenine dinucleotide (BaAD). The unbiased electron density of the BaAD compound is clear and allowed unambiguous identification of the new chemical entity and its interaction with the S1. The respective positions of the ADP-ribose and the abutting h2 helix show significant differences compared to the pre- and post-NAD hydrolysis structures ($S1_{NAD}$ and $S1_{ADPR/NA}$, respectively) with the binding mode of BaAD sharing elements of both states.

The co-factor for S1 is β-NAD$^+$ in which the nicotinamide adjacent sugar adopts the physiologically dominant β-D-ribose configuration. Within our pre-NAD+ hydrolysis structures, this configuration is clear (Fig. 4*D*). Within our post-NAD+ hydrolysis $S1_{APDR/NA}$ structure, this sugar has clearly converted to an α-D-ribose due to the orientation of the C1′ hydroxyl (Fig. 4*D*). The N-ribose rotates significantly during transition between the $S1_{NAD}$ and postreaction $S1_{ADPR/NA}$ states. The formation of the BaAD compound from 3AB results in an N-ribose position midway between these two states (Fig. 4*D*). We propose that the formation of BaAD by S1 proceeds through the canonical oxocarbenium cation transition state (Fig. 4*C*, see Discussion for details).

The structural flexibility of S1 facilitates induced-fit inhibitor binding

6(5H)-Phenanthridinones are tricyclic γ-Lactam compounds known to inhibit poly ADP ribose polymerase (PARP) enzymes (41) and bacterial ARTs (42, 43) including those similar to PT with micromolar Ki (44). When bound within PARP-1, the benzamide backbone of such molecules acts as a competitive inhibitor occupying their nicotinamide sites. The ADP-ribosylation activity of S1 against Gαi is reduced to 50 to 25% in the presence of millimolar concentrations of N-(5,6-dihydro-6-oxo-2-phenanthridinyl)-2-(dimethylamino)acetamide (PJ34) (Fig. 5*A*). To investigate this binding mode, we co-complexed PJ34 with the S1 subunit (C41S mutant) and obtained its structure (referred to as S1PJ34) (Fig. 5*B*). The benzamide backbone of PJ34 was seen to bind within the nicotinamide site as expected, positioning the planar tricyclic ring system such that the second aromatic ring base stacks against Arg-9 in place of its interaction with the NAD+ phosphates. In contrast, the subsites for the adenine moiety of NAD+ and its two ribose sugars remain unoccupied. The decorating dimethylamino acetamide group of PJ34 projects out of the standard NAD+-binding groove, abutting the C-terminus of h2. However, the position of h2 in this PJ34-bound state is not contracted into its active conformation (Fig. 5*C*) and is more similar to the inactive S1APO state than the more compact active one. Thus, the inherent flexibility of S1 allows it to bind PARP inhibitors even when they incompletely fill the nucleotide-binding site. The PJ34-binding mode within S1 is similar to that within Scabin toxin for which the compound is an effective inhibitor (44), particularly over the nicotinamide-like portion of the molecule (Fig. 5*D*). However, in Scabin, residues within the active site loop further facilitate its binding by contributing additional interactions. These interactions are missing within S1PJ34 (Fig. 5*C*) despite the presence of a similar residue within the loop (Gln-42) and the dimethylamino-acetamide group is excluded from the S1 adenine-binding cleft.

Discussion

We describe crystal structures of the S1 subunit of PT in complex with NAD+, with ADP-ribose and nicotinamide, with

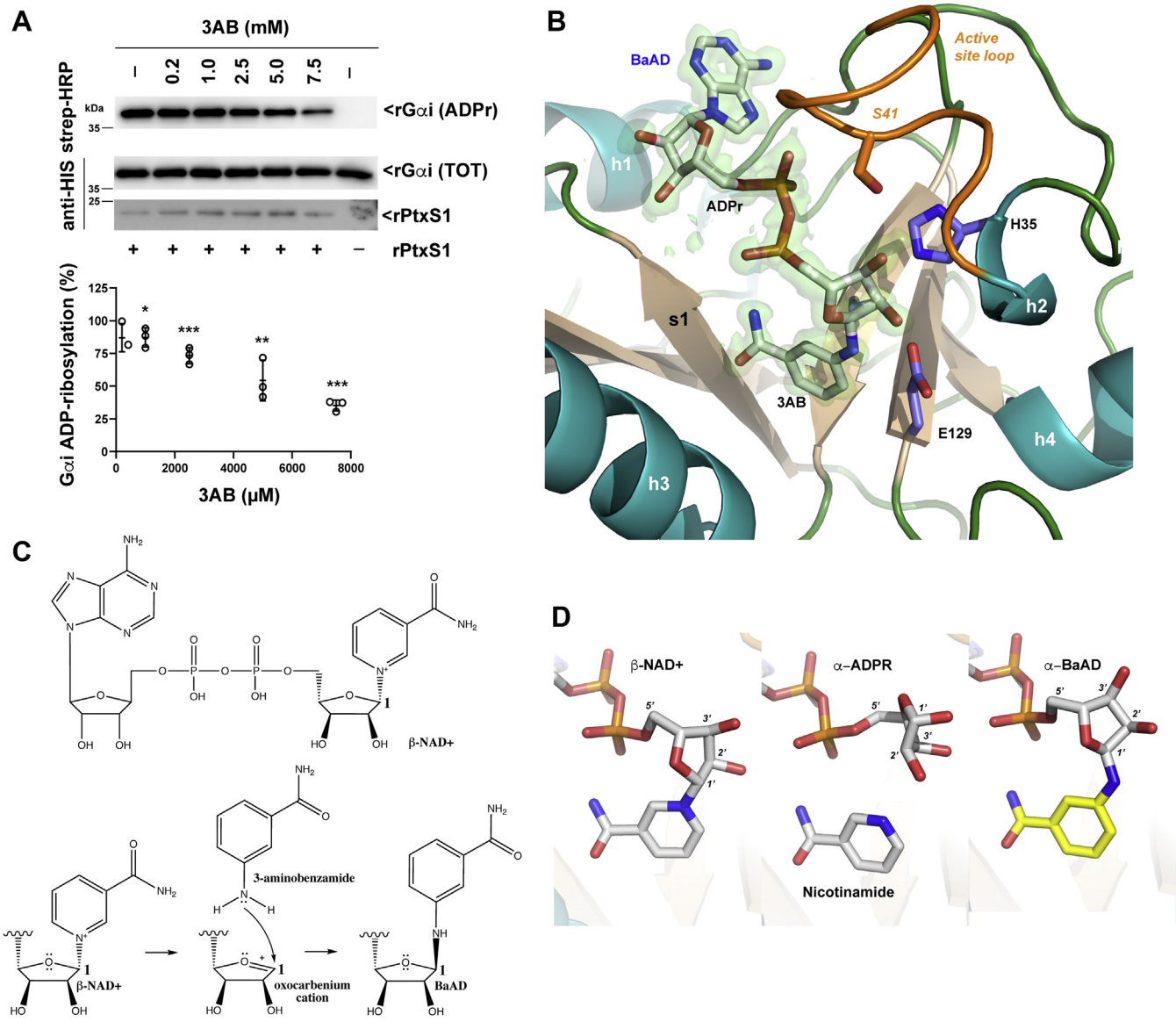

Figure 4. BaAD forms within PT S1 from 3AB and NAD+. *A*, effect of 3AB on Gαi-targeted ADP-ribosyltransferase activity of S1. *In vitro* ADP-ribosylation assay was done with recombinant S1 (rPtxS1), recombinant Gαi (rGαi), biotin-NAD+, and 3AB at different concentrations. The rGαi-conjugated biotin-ADP-ribose was detected with streptavidin-HRP. The same samples were analyzed in two parallel membranes, that is, strep-HRP and anti-HIS (with two exposure lengths). Quantitation of rGαi ADP-ribosylation in three independent experiments (% of pixel intensity as compared to the sample without inhibitor) is shown with a scatterplot (**p*-value <0.05; ***p*-value <0.01; ****p*-value <0.005, Student's *t* test two-sample equal variance). *B*, cartoon representation of the BaAD transition-state inhibitor within the NAD-binding site of S1. Colors used are consistent with Figure 1. The partially transparent green surface represents a 3.0-σ omit map contour prior to inclusion of the compound during refinement. The position of key residues is shown using stick representation. *C*, potential reaction scheme for the formation of BaAD within the S1 catalytic site. *D*, when the protein subunits of the $S1_{NAD}$, $S1_{ADPR}$, and $S1_{3AB}$ structures are aligned, a stick representation of the N-ribose displays the movement experienced at different reaction states. 3AB, 3-amino benzamide; BaAD, benzamide amino adenine dinucleotide; HRP, horseradish peroxidase; NAD+, nicotinamide adenine dinucleotide; PT, pertussis toxin.

NAD+ analog PJ34, and with a novel NAD+ analog termed here as BaAD formed upon S1 subunit crystallization with 3AB and NAD+. These crystal structures represent the first nucleotide-bound forms of PT and therefore provide unprecedented insights into pre- and post-NAD+ hydrolysis steps of the ART activity of PT.

Dissociation of the inhibitory C-terminal residues following reduction of the intramolecular disulfide in S1, mimicked in this study by genetic means, results in considerable lobe closure about the nucleotide upon activation. These activation-induced structural changes of S1 are globally similar to those described for the orthologous *Escherichia coli* toxin *Ec*Plt (23). In contrast, the activation mechanism of cholera toxin deploys a predominant loop-refolding mechanism in which its two lobes remain static (45). After dissociation of the inhibitory C-terminal residues, the active-site loop in S1 is able to fold over the phosphate groups and A-ribose firmly clamps the ADP section of NAD^+. A nucleotide clamp is a common feature of ART enzymes (46); it has been proposed that enzymatic activity may be catalyzed through simultaneously fixing the adenine base while inducing a compact conformation within the other end of the molecule near the nicotinamide, N-ribose and N-phosphate (34). The catalytic glutamate then draws

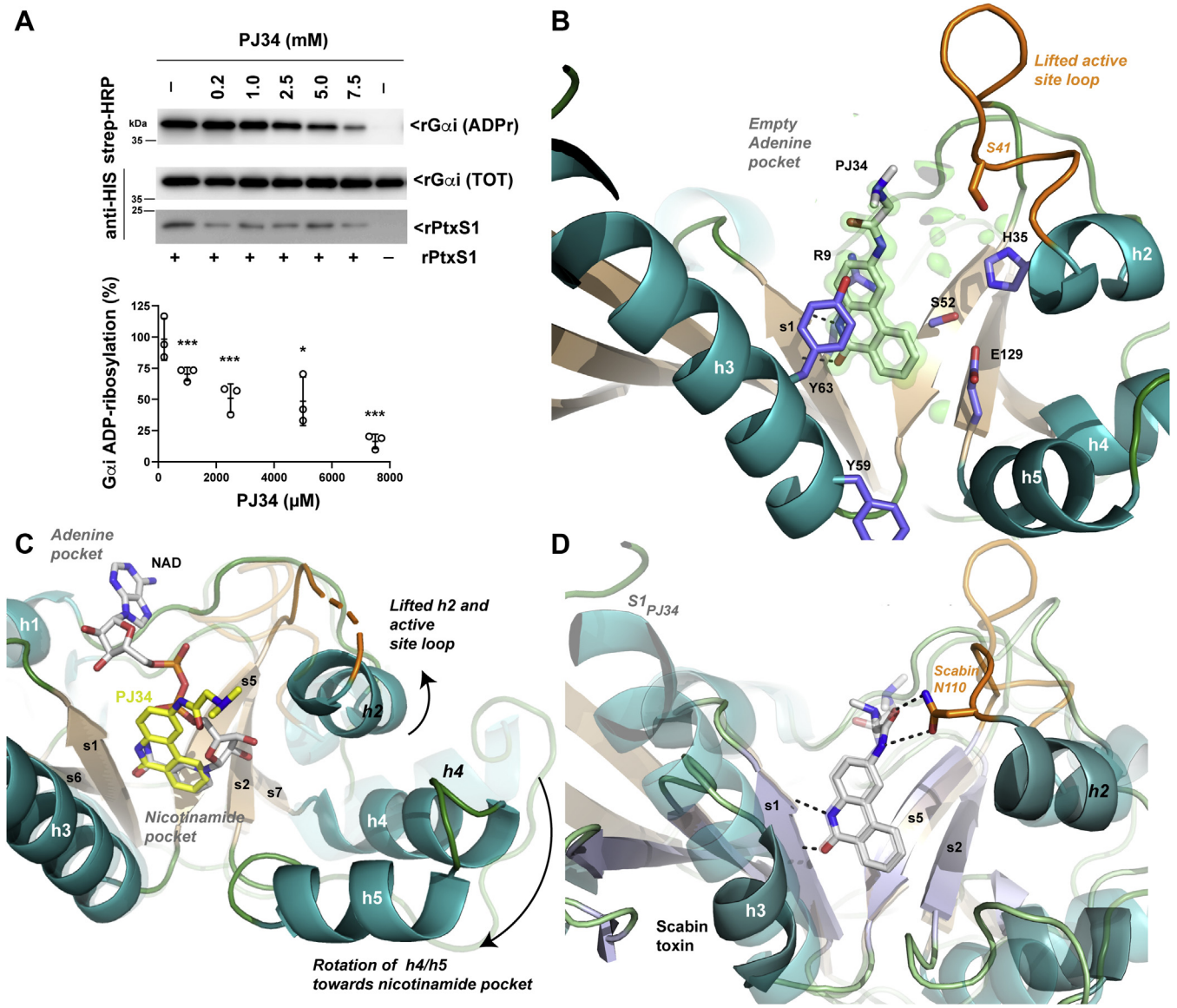

Figure 5. PJ34 binds within PT S1. *A*, effect of PJ34 on Gαi-targeted ADP-ribosyltransferase activity of S1. *In vitro* ADP-ribosylation assay was done with recombinant S1 (rPtxS1), recombinant Gαi (rGαi), biotin-NAD+, and PJ34 at different concentrations. The rGαi-conjugated biotin-ADP-ribose was detected with streptavidin-HRP. The same samples were analyzed in two parallel membranes, that is, strep-HRP and anti-HIS (with two exposure lengths). Quantitation of rGαi ADP-ribosylation in three independent experiments (% of pixel intensity as compared to the sample without inhibitor) is shown with a scatterplot (**p*-value <0.05; ***p*-value <0.01; ****p*-value <0.005, Student's *t* test two-sample equal variance). *B*, cartoon representation of the PARP1 inhibitor PJ34 bound within S1. Colors used are consistent with Figure 1. The partially transparent green surface represents a 3.6-σ omit map contour prior to inclusion of the compound during refinement. The position of key residues is shown using stick representation. *C*, alignment of $S1_{PJ34}$ with that of $S1_{NAD}$ highlights the movements within key regions of the protein (h2, h4, h5, and the active site loop). *D*, when $S1_{PJ34}$ (partially transparent) is compared with PJ34-bound Scabin (PDB 5EWK, (44)), the degree of conservation of the inhibitor-binding site can be observed. HRP, horseradish peroxidase; NAD+, nicotinamide adenine dinucleotide; PJ34, N-(5,6-dihydro-6-oxo-2-phenanthridinyl)-2-(dimethylamino)acetamide; PT, pertussis toxin.

electrons onto the ribose ring, weakening the N-glycosidic bond. This promotes lysis and formation of a highly strained oxocarbenium intermediate (34). The enzyme's adenine/phosphate clamp forces strain relief onto the N-ribose such that it rotates to create a second oxocarbenium intermediate. In iota toxin, strain relief occurs through rotation of both the N-phosphate and N-ribose of the nucleotide prior to formation of an ADP-ribosylated actin (34). Our $S1_{ADPR/NA}$ structure implies that movement of the N-phosphate in S1 is restricted by Tyr-63, so strain relief is forced entirely into rotation of the N-ribose sugar, and this moves the anomeric carbon ~4 Å toward helix 2 whose dipole moment may stabilize the charge on the oxocarbenium prior to nucleophilic attack by the G protein substrate.

As part of attempts to develop a safe genetically inactivated PT vaccine, *B. pertussis* strains expressing E129D, E129Q, or E129G mutations were shown to display reduced virulence and ART activity, yet still elicit protective immune responses (47). Our ART activity assays concur with prior work demonstrating that E129 is essential for the catalytic activity of S1 (47–50) and that C41S mutants have minimal effect (37, 51). Our structures help provide a framework to detail why such mutations inactivate the protein. Within our $S1_{E129D}$ structure, the interaction between the negative charge of Glu-129 and the

N-ribose ring of NAD^+ is disrupted as it is displaced toward solvent. Thus, catalytic activity is obviously dependent on precise positioning of the carboxyl group of Glu-129, a fact highlighted through the unexpected inactivating effect of iodide ions that also serve to displace this negative charge. R9K mutations are known to inactivate S1 (47); our structure shows that its guanidinium group interacts with both NAD+ phosphates as previously predicted.

The ART activity of PT is dependent on other key residues within the S1 subunit; Ser-52 or His-35 mutations both reduce activity compared to the wildtype protein (52). The entire active-site loop of PT folds over the NAD^+ phosphates, ensuring complete enclosure of the binding site; the equivalent loop within cholera toxin leaves its active site more open (45). In the $S1_{E129D}$ and $S1_{ADPR/NA}$ structures, His-35, Ser-52, and Glx-129 form a network of hydrogen bonds that provide one of the few stabilizing interactions for the catalytically permissive position of the Glu-129 carboxyl group. Given they can be mutated without completely abrogating activity (52) a primary role for these residues may be stabilization of the catalytically permissive position of Glu-129 and the movements of h2 during catalysis.

The reduced *apo* S1 subunit is reported to be a thermally unstable protein prone to proteolysis, which becomes more stable following NAD^+ binding (29). B-subunit dissociation from S1 may thus lead to a form with a number of conformational states, and NAD^+ promotes the formation of the enzymatically active forms we see in our crystals which still display considerable heterogeneity. In S1, the loop preceding the catalytic glutamate is larger than that of other ARTs. Following release from the pseudopentamer residues 112 to 129 appears to become inherently moldable, we observed at least six different conformations within our crystal structures spanning the range of those that retain all or half of the h5 helix, while others loose it entirely along with the last turn of h4. On a microfocus beamline, the structures adopted by the loop could differ in data collected on the one side of a crystal compared to that of the other. This loop may become more ordered upon binding to G proteins, potentially suggesting an entropic component to binding. Our alphafold2 models highlighted this possibility with this region of the protein binding near $G_{\alpha i}$-α5 in an ICL2-like position. However, a number of potential docking modes were computed; those exposing the hydrophobic face of the last three turns of the $G_{\alpha i}$-α5 helix are consistent with our observed reduction in activity for the Y59A and Y63A S1 mutants as well as the lack of an effect of V62Y and S56Q. Our substrate GNAI3 C-terminal mutants are broadly consistent with those published elsewhere on GNAO using radiolabeled substrate (53); both sets of experiments show C351S mutants cannot act as a substrate, while L353A shows reduced activity. Our work implies the Y354Δ mutant may compromise the role of GNAI3 as a substrate more than that of GNAO (53). Further mutational work is required to rigorously test such results.

Small-molecule ART inhibitors have been developed as a means to inhibit PT (18) and PARPs (54). We therefore sought to investigate how such compounds could act on S1. Most known compounds act as competitive inhibitors and are based around an amide-like group that anchors within the conserved ART nicotinamide-binding pocket, and molecular extensions are then used to increase affinity and/or specificity. One of the first such compounds discovered was 3AB which is a relatively minimal nicotinamide mimic that is clinically well tolerated (55). Due to its simple form, 3AB is nonspecific and inhibits a range of mono(ADP-ribosyl) transferase and PARP enzymes with micromolar K_i (56). We observed a relatively high millimolar inhibition of S1-catalyzed Gαi ADP-ribosylation. The 3AB-bound structures of human PARP2 (57), PARP10, PARP14 (58) and PARP16 (59) had previously indicated a common binding mechanism in which the benzamide of 3AB occupies each enzyme's respective nicotinamide-binding site; the inhibitor's aromatic nitrogen provides no more than an additional van der Waals contact to nearby aromatic residues. To our knowledge, all previous 3AB-inhibited ART structures have been obtained in the absence of adenine dinucleotide compounds such as NAD^+ or ADP-ribose, whereas the enzymatic assays used to determine their inhibitory potential obviously contain them. The ADP-ribosylation reaction in S1 is thought to proceed *via* an SN_1 reaction scheme that produces metastable oxocarbenium intermediates with the potential for forming novel drug adjuncts (60–62). In our study, we witnessed the formation of a novel NAD+ analog, termed BaAD.

We propose that the formation of BaAD by S1 proceeds through an oxocarbenium cation transition state (see Fig. 4*C*). PtxS1/β-NAD+-complex would first undergo activation of β-NAD+ to form the oxocarbenium cation, with Glu-129 having a major catalytic role. Next, nucleophilic attack of the electrophilic ribose C1 carbon would happen by the nitrogen atom of the 3AB amine group. This reaction scheme mimics what happens at the catalytic center of S1 in the presence or absence of the Gαi substrate. Formation of the oxocarbenium cation transition state has been witnessed in S1 in both of these catalytic conditions prior the nucleophilic attack either by the sulfur atom of cysteine side chain of Gαi or by oxygen atom of the water molecule (60–62). It is also remarkable that we witnessed an α-configuration in how the aniline nitrogen of 3AB is linked to ribose. This indicates that the formation of BaAD by S1 involves the canonical stereospecific ART-catalyzed reaction scheme producing α-ADP-ribosyl linkages from β-NAD+ (*e.g.*, (63–65). Our structural data also support the stereospecific ART activity of S1 (see Fig. 4*D*).

As the formation of BaAD became obvious only once we obtained our 1.0-Å resolution co-complex structure, a rarely achieved resolution, the question arises: is this inhibitory mechanism more universal but not previously detected? It is possible that ART activity against small molecules may be a more general feature of ART enzymes that could serve to create inhibitors with a higher affinity than the parent compound. Alternatively, the structurally highly flexible nature of S1 may make it particularly susceptible to BaAD formation in a way that other enzymes are not. Both possibilities should be kept in mind when analyzing the binding modes of ART inhibitors; otherwise, affinity and structural data may become

disconnected from the actual mechanism of inhibition. Current ART-inhibitor design focuses on creating molecules with affinity for the NAD^+ cleft itself; if the mechanism we detail is more universal, it may also be possible to utilize small "prodrugs"-like compounds that initially bind within the nicotinamide pocket and maybe extend out to the protein substrate-binding site. Their subsequent ADP-ribosylation *in vivo* could then serve as a means to create transition-state analog with higher affinity.

Experimental procedures

Cloning

A codon-optimized gene encoding the S1 subunit of *B. pertussis* strain Tohama I (Uniprot_P04977) or human GNAI3 (Uniprot_P08754) was synthesized and cloned into a pET28-derived vector, yielding proteins fused to a hexahistidine tag through a human rhinovirus 3C (HRV 3C) cleavage site. The S1 constructs cloned encompassed residues S1(D35-R256). The GNAI3 constructs encompassed residues V34-Y354. For enzymatic assays, single-site mutants were incorporated into these constructs using a high-fidelity polymerase chain reaction followed by DpnI digestion of the parental vector. All constructs were confirmed by sequencing.

Protein production

For protein expression, S1 constructs were transformed into BL21 (DE3) *E. coli* cells which were grown at 37 °C in LB medium supplemented with 30 μg/ml kanamycin. After reaching an absorption A_{600nm} of 0.6 to 0.8, the temperature was dropped to 18 °C and the cells were induced for 18 h with 0.2 mM of isopropyl β-D-1-thiogalactopyranoside. Cells were harvested and resuspended in 20 mM Hepes, pH 7.0, 250 mM NaCl, 20 mM imidazole, 1 mM tris(2-carboxyethyl)phosphine (TCEP) and then lysed by adding 1 mg/ml lysozyme and DNase and sonicated. Cleared lysate was applied to a Ni-NTA affinity column and washed extensively before eluting in 20 mM Hepes, pH 7.0, 250 mM NaCl, 400 mM imidazole, 1 mM TCEP. The protein's hexahistidine tag was removed by incubating the eluted protein with 0.1 mg/ml GST-fused HRV 3C overnight at 4 °C. Following cleavage, the HRV 3C protease was removed by passing over 0.1 ml of agarose resin with the flow and subsequently purified by gel filtration on an Superdex S75 16/60 (GE Healthcare Life Sciences). The constructs eluted as a single peak corresponding to monomeric S1. Expression of the different *Hs*GNAI3 constructs was identical to that of S1 except they required 0.01% v/v Triton x100 during HRV 3C cleavage and the protein was transferred into 20 mM Hepes, 50 mM NaCl, and 1 mM TCEP to allow an additional HiTrap Q purification column prior to gel filtration.

Enzymatic assays

The activity of different S1 constructs was monitored using 6-Biotin-17-NAD^+ (BPS Biosciences #80610) as a substrate that could then be visualized using StrepTactin-conjugated horseradish peroxidase (HRP; Bio-RAD #161-0381). Briefly each reaction mix contained 1 μM of recombinant *Hs*GNAI3 substrate. The G proteins in 50 mM Hepes, pH 7.0, 140 mM NaCl, 20 mM DTT, and 50 μM Biotin-NAD was incubated for 5 min at 37 °C with 20 nM of purified recombinant S1. Reactions were stopped by adding SDS-loading buffer and heating at 100 °C for 5 min before running on SDS-PAGE and transferring to a nitrocellulose membrane prior to being visualized using StrepTactin-HRP and Pierce chemiluminescence substrate. Full-sized versions of the blots and loading controls are presented in Fig. S4.

Enzymatic inhibitor assays

Reactions (in 50 μl) contained 100 nM of N-terminally HIS-tagged S1 and 1 μM Gαi, purified as described (18), in 100 mM Hepes (pH 7.5), 500 mM NaCl, and 10% (w/v) glycerol and 2 μM biotinylated NAD^+ (Trevigen, 4670–500–01). The reactions were carried out at room temperature for 40 min. For validating the inhibitory effect of PJ34 and 3AB, a range of concentrations (200, 1000, 2500, 5000, and 7500 μM) of the indicated compound (and H_2O in control reaction) was used. Inhibitory compounds were incubated for 5 min with S1 prior to adding rest of the reaction components. Reactions were stopped by addition of Laemmli loading dye to 1 × and heating for 5 min at 95 °C. The proteins were separated in SDS-PAGE and transferred to nitrocellulose membrane, followed by membrane blocking with 1% (w/v) casein blocking buffer (Bio-Rad, 161-0782). Membranes were incubated with streptavidin conjugated to HRP (1:5000) (GE Healthcare, RPN1231VS) in 1% (w/v) casein blocking buffer (Bio-Rad, 161-0782) for 3 h at 4 °C in rotation and washed thrice with Tris-buffered saline (10 mM Tris-HCl [pH 7.5], 150 mM NaCl) containing 0.05% Tween 20 (TBST) for 10 min each time. Alternatively, after blocking with 5% (w/v) nonfat milk in TBST, membranes were probed in TBST containing 5 % (w/v) nonfat milk (24–48 h at 4 °C in rotation) for HIS-tagged rPtxS1 and rGαi proteins with mouse monoclonal anti-HIS (1:1000) (R&D Systems, MAB050). Primary antibody membranes were washed thrice with TBST containing 5% (w/v) nonfat milk for 10 min each time. Primary antibody membranes were incubated with mouse IgG kappa–binding protein conjugated to HRP (1:2500) (sc-516102, Santa Cruz Biotechnology) in 5% (w/v) nonfat milk TBST for 3 h at 4 °C in rotation and washed thrice with TBST for 10 min each time. All membranes were subsequently developed with Western-Bright ECL (Advansta) and imaged on ImageQuant LAS 4000 (GE Healthcare). Pixel intensities were quantified from the Western blot TIFF files using ImageJ 1.44o (NIH, USA, https://imagej.nih.gov/ij/). For the quantitation of the inhibitory effect of PJ34 and 3AB on S1-catalyzed ADP-ribosylation of Gαi, the pixel intensities of the streptavidin-HRP signal were normalized based on the control sample, that is, the sample without an added inhibitor. Full-sized versions of the blots and loading controls are presented in Fig. S5.

Crystallization

Crystals of $S1_{NAD}$ and $S1_{E129D}$ bound to NAD^+ (Sigma-Aldrich N7004) were obtained by incubating protein at 8 to

10 mg/ml with 1 mM NAD^+ for 10 min before setting up as hanging drops in a 1:1 ratio over a reservoir of 25% PEG 3350, 0.2 M potassium iodide. Crystal clusters grew in 6 to 12 days and were crushed to use as seeds to obtain single crystals. Crystals were transferred into cryoprotectant consisting of 25% v/v glycerol prior to plunging into liquid nitrogen. To obtain $S1_{ADPR/NA}$ crystals, the S1(C41S) was complexed with 1 mM NAD+ and crystallized over the physiologically permissive solution 0.5 M $(NH_4)_2SO_4$ and 0.1 M Hepes, pH 7. Cryoprotectant consisted of an additional 25% v/v glycerol, added to the reservoir. The structure of $S1_{AB}$ was obtained when S1(C41S) was co-complexed with both 1 mM NAD^+ and 1 mM 3AB. Crystals were grown in 0.2 M LiCl and 14% w/v PEG 3350 and transferred to a cryoprotectant solution with an additional 27% v/v glycerol prior to data collection. The structure of $S1_{PJ34}$ was obtained when S1(C41S) was co-complexed 1 mM PJ34 and crystallized over a reservoir containing 0.15 M NaCl, 0.1 M Tris(hydroxymethyl)aminomethane, pH 8.0, and 8% w/v PEG 8000. Crystals were soaked into a solution with an additional 25% v/v glycerol before flash freezing in liquid nitrogen.

Data collection and structure solution

All diffraction data were collected at 100K at the Australian Synchrotron MX1 and MX2 beamlines. The S1 crystals were highly layered, diffracted well, but had split reflections in large beams. Most of our S1 datasets appear to diffract in P4, but processing in P1 was found to be preferential due to variation within the h5 helical residues. The conformation of these residues would vary across regions of a single crystal, making the microfocus beamline preferred for collection. Despite this crystal pathology, diffraction resolution was good and electron density maps looked clear provided the crystals were well fragmented and carefully shot. Data collection and refinement statistics are presented in Table S1, and the space group P1 was enforced on all but the $S1_{PJ34}$ and $S1_{E129D}$ data. A trimmed version of the S1 subunit from the inactive PT holotoxin (PDB code 1BCP (27)) was used as an initial molecular replacement probe in the program Phaser (66). The resulting electron density highlighted sections of the structure with altered conformation upon activation, these sections were deleted from the model, and the maps were recalculated. The model was then improved by simulated annealing and rounds of manual building and refinement using the programs COOT (67) and PHENIX (68).

Alphafold2 modeling

The S1 sequence including C41S, S52E mutations was computationally folded with the C-terminus of different Gαi sequences using alphafold2 (39). Gmini sequences of Gαi were preferred for modeling as this reduced computational loads. After modeling was completed, the crystallographically obtained nucleotide-bound forms of S1 were overlaid upon the computational model to provide positioning of the NAD+ within the context of the substrate-docked toxin. The S52E mutation was used to mimic NAD hydroxyls.

Data availability

The atomic coordinates and observed structure factors have been deposited in the Research Collaboratory for Structural Bioinformatics Protein Data Bank (PDB) with codes 7SKY, 7U6Z, 7SKK, 7SNE, and 7SKI.

Supporting information—This article contains supporting information.

Funding and additional information—This research was undertaken in part using the MX1 beamline at the Australian Synchrotron, part of ANSTO. J. R. is an NHMRC Fellow. The exotoxin research in the laboratory of Arto Tapio Pulliainen (A. T. P.) has received financial support from Academy of Finland (grants no. 295296 and 329252, to A. T. P.), Sigrid Juselius Foundation (to A. T. P.), Instruct ERIC (to A. T. P.), the Finnish Society of Sciences and Letters (to A. T. P.), University of Turku, Turku, Finland (to A. T. P.), Turku Doctoral Programme of Molecular Medicine (TuDMM) (to Moona Sakari, M. S.), the Finnish Cultural Foundation (to M.S.), and Turku University Foundation (to M.S.). The funders have had no role in study designs, data collection and interpretations, or the decisions to submit the results for publication.

Author contributions—D. R. L., T. B, A. T. P., and J. R. conceptualization; D. R. L., T. B., and A. T. B funding acquisition; D. R. L., M. T. T., and M. S. investigation; D. R. L., T. B, A. T. P., and J. R. supervision; D. R. L. validation; D. R. L., T. B, A. T. P., and J. R. writing – review and editing.

Conflict of interest—The authors declare that they have no conflicts of interest.

Abbreviations—The abbreviations used are: 3AB, 3-amino benzamide; ART, ADP-ribosyltransferase; BaAD, benzamide amino adenine dinucleotide; ER, endoplasmic reticulum; HRP, horseradish peroxidase; NAD+, nicotinamide adenine dinucleotide; PARP, poly ADP ribose polymerase; PJ34, N-(5,6-dihydro-6-oxo-2-phenanthridinyl)-2-(dimethylamino)acetamide; PT, pertussis toxin; TCEP, tris(2-carboxyethyl)phosphine.

References

1. Kilgore, P. E., Salim, A. M., Zervos, M. J., and Schmitt, H. J. (2016) Pertussis: Microbiology, disease, treatment, and prevention. *Clin. Microbiol. Rev.* **29**, 449–486
2. Ulloa-Gutierrez, R., Boza, R., Carvajal-Riggioni, D., and Baltodano, A. (2011) Pertussis: Should we improve intensive care management or vaccination strategies? *Expert Rev. Vaccin.* **10**, 49–53
3. von Konig, C. H., Halperin, S., Riffelmann, M., and Guiso, N. (2002) Pertussis of adults and infants. *Lancet Infect. Dis.* **2**, 744–750
4. Mooi, F. R., NA, V. D. M., and De Melker, H. E. (2013) Pertussis resurgence: Waning immunity and pathogen adaptation - two sides of the same coin. *Epidemiol. Infect.* **142**, 1–10
5. Phadke, V. K., Bednarczyk, R. A., Salmon, D. A., and Omer, S. B. (2016) Association between vaccine refusal and vaccine-preventable diseases in the United States: A review of measles and pertussis. *JAMA* **315**, 1149–1158
6. Carbonetti, N. H., Artamonova, G. V., Van Rooijen, N., and Ayala, V. I. (2007) Pertussis toxin targets airway macrophages to promote Bordetella pertussis infection of the respiratory tract. *Infect. Immun.* **75**, 1713–1720
7. Kirimanjeswara, G. S., Agosto, L. M., Kennett, M. J., Bjornstad, O. N., and Harvill, E. T. (2005) Pertussis toxin inhibits neutrophil recruitment to

delay antibody-mediated clearance of Bordetella pertussis. *J. Clin. Invest.* **115**, 3594–3601
8. Scanlon, K., Skerry, C., and Carbonetti, N. (2019) Association of pertussis toxin with severe pertussis disease. *Toxins (Basel)* **11**, 373
9. Pittman, M. (1984) The concept of pertussis as a toxin-mediated disease. *Pediatr. Infect. Dis.* **3**, 467–486
10. Tuomanen, E., and Weiss, A. (1985) Characterization of two adhesins of Bordetella pertussis for human ciliated respiratory-epithelial cells. *J. Infect. Dis.* **152**, 118–125
11. Hall, E., Parton, R., and Wardlaw, A. C. (1994) Cough production, leucocytosis and serology of rats infected intrabronchially with Bordetella pertussis. *J. Med. Microbiol.* **40**, 205–213
12. Parton, R., Hall, E., and Wardlaw, A. C. (1994) Responses to Bordetella pertussis mutant strains and to vaccination in the coughing rat model of pertussis. *J. Med. Microbiol.* **40**, 307–312
13. Mooi, F. R., van Loo, I. H., van Gent, M., He, Q., Bart, M. J., Heuvelman, K. J., de Greeff, S. C., Diavatopoulos, D., Teunis, P., Nagelkerke, N., and Mertsola, J. (2009) Bordetella pertussis strains with increased toxin production associated with pertussis resurgence. *Emerging Infect. Dis.* **15**, 1206–1213
14. Yeh, S. H. (2003) Pertussis: Persistent pathogen, imperfect vaccines. *Expert Rev. Vaccin.* **2**, 113–127
15. Sato, H., and Sato, Y. (1984) Bordetella pertussis infection in mice: Correlation of specific antibodies against two antigens, pertussis toxin, and filamentous hemagglutinin with mouse protectivity in an intracerebral or aerosol challenge system. *Infect. Immun.* **46**, 415–421
16. Sakari, M., Laisi, A., and Pulliainen, A. T. (2022) Exotoxin-targeted drug modalities as antibiotic alternatives. *ACS Infect. Dis.* **8**, 433–456
17. Nguyen, A. W., Wagner, E. K., Laber, J. R., Goodfield, L. L., Smallridge, W. E., Harvill, E. T., Papin, J. F., Wolf, R. F., Padlan, E. A., Bristol, A., Kaleko, M., and Maynard, J. A. (2015) A cocktail of humanized anti-pertussis toxin antibodies limits disease in murine and baboon models of whooping cough. *Sci. Transl Med.* **7**, 316ra195
18. Ashok, Y., Miettinen, M., Oliveira, D. K. H., Tamirat, M. Z., Nareoja, K., Tiwari, A., Hottiger, M. O., Johnson, M. S., Lehtio, L., and Pulliainen, A. T. (2020) Discovery of compounds inhibiting the ADP-ribosyltransferase activity of pertussis toxin. *ACS Infect. Dis.* **6**, 588–602
19. Ernst, K., Mittler, A. K., Winkelmann, V., Kling, C., Eberhardt, N., Anastasia, A., Sonnabend, M., Lochbaum, R., Wirsching, J., Sakari, M., Pulliainen, A. T., Skerry, C., Carbonetti, N. H., Frick, M., and Barth, H. (2021) Pharmacological targeting of host chaperones protects from pertussis toxin *in vitro* and *in vivo*. *Sci. Rep.* **11**, 5429
20. Stein, P. E., Boodhoo, A., Armstrong, G. D., Cockle, S. A., Klein, M. H., and Read, R. J. (1994) The crystal structure of pertussis toxin. *Structure* **2**, 45–57
21. Stein, P. E., Boodhoo, A., Armstrong, G. D., Heerze, L. D., Cockle, S. A., Klein, M. H., and Read, R. J. (1994) Structure of a pertussis toxin-sugar complex as a model for receptor binding. *Nat. Struct. Biol.* **1**, 591–596
22. Song, J., Gao, X., and Galan, J. E. (2013) Structure and function of the Salmonella Typhi chimaeric A(2)B(5) typhoid toxin. *Nature* **499**, 350–354
23. Littler, D. R., Ang, S. Y., Moriel, D. G., Kocan, M., Kleifeld, O., Johnson, M. D., Tran, M. T., Paton, A. W., Paton, J. C., Summers, R. J., Schembri, M. A., Rossjohn, J., and Beddoe, T. (2017) Structure-function analyses of a pertussis-like toxin from pathogenic Escherichia coli reveal a distinct mechanism of inhibition of trimeric G-proteins. *J. Biol. Chem.* **292**, 15143–15158
24. Sixma, T. K., Pronk, S. E., Kalk, K. H., Wartna, E. S., van Zanten, B. A., Witholt, B., and Hol, W. G. (1991) Crystal structure of a cholera toxin-related heat-labile enterotoxin from E. coli. *Nature* **351**, 371–377
25. Plaut, R. D., and Carbonetti, N. H. (2008) Retrograde transport of pertussis toxin in the mammalian cell. *Cell Microbiol.* **10**, 1130–1139
26. Plaut, R. D., Scanlon, K. M., Taylor, M., Teter, K., and Carbonetti, N. H. (2016) Intracellular disassembly and activity of pertussis toxin require interaction with ATP. *Pathog. Dis.* **74**, ftw065
27. Hazes, B., Boodhoo, A., Cockle, S. A., and Read, R. J. (1996) Crystal structure of the pertussis toxin-ATP complex: A molecular sensor. *J. Mol. Biol.* **258**, 661–671
28. Banerjee, T., Cilenti, L., Taylor, M., Showman, A., Tatulian, S. A., and Teter, K. (2016) Thermal unfolding of the pertussis toxin S1 subunit facilitates toxin translocation to the cytosol by the mechanism of endoplasmic reticulum-associated degradation. *Infect. Immun.* **84**, 3388–3398
29. Pande, A. H., Moe, D., Jamnadas, M., Tatulian, S. A., and Teter, K. (2006) The pertussis toxin S1 subunit is a thermally unstable protein susceptible to degradation by the 20S proteasome. *Biochemistry* **45**, 13734–13740
30. Ernst, K., Eberhardt, N., Mittler, A. K., Sonnabend, M., Anastasia, A., Freisinger, S., Schiene-Fischer, C., Malesevic, M., and Barth, H. (2018) Pharmacological cyclophilin inhibitors prevent intoxication of mammalian cells with Bordetella pertussis toxin. *Toxins (Basel)* **10**, 181
31. West, R. E., Jr., Moss, J., Vaughan, M., Liu, T., and Liu, T. Y. (1985) Pertussis toxin-catalyzed ADP-ribosylation of transducin. Cysteine 347 is the ADP-ribose acceptor site. *J. Biol. Chem.* **260**, 14428–14430
32. Carbonetti, N. H., Mays, R. M., Artamonova, G. V., Plaut, R. D., and Worthington, Z. E. (2005) Proteolytic cleavage of pertussis toxin S1 subunit is not essential for its activity in mammalian cells. *BMC Microbiol.* **5**, 7
33. Menetrey, J., Flatau, G., Boquet, P., Menez, A., and Stura, E. A. (2008) Structural basis for the NAD-hydrolysis mechanism and the ARTT-loop plasticity of C3 exoenzymes. *Protein Sci.* **17**, 878–886
34. Tsurumura, T., Tsumori, Y., Qiu, H., Oda, M., Sakurai, J., Nagahama, M., and Tsuge, H. (2013) Arginine ADP-ribosylation mechanism based on structural snapshots of iota-toxin and actin complex. *Proc. Natl. Acad. Sci. U. S. A.* **110**, 4267–4272
35. Isom, D. G., Castaneda, C. A., Cannon, B. R., Velu, P. D., and Garcia-Moreno, E. B. (2010) Charges in the hydrophobic interior of proteins. *Proc. Natl. Acad. Sci. U. S. A.* **107**, 16096–16100
36. Locht, C., Capiau, C., and Feron, C. (1989) Identification of amino acid residues essential for the enzymatic activities of pertussis toxin. *Proc. Natl. Acad. Sci. U. S. A.* **86**, 3075–3079
37. Locht, C., Lobet, Y., Feron, C., Cieplak, W., and Keith, J. M. (1990) The role of cysteine 41 in the enzymatic activities of the pertussis toxin S1 subunit as investigated by site-directed mutagenesis. *J. Biol. Chem.* **265**, 4552–4559
38. Domenighini, M., and Rappuoli, R. (1996) Three conserved consensus sequences identify the NAD-binding site of ADP-ribosylating enzymes, expressed by eukaryotes, bacteria and T-even bacteriophages. *Mol. Microbiol.* **21**, 667–674
39. Jumper, J., Evans, R., Pritzel, A., Green, T., Figurnov, M., Ronneberger, O., Tunyasuvunakool, K., Bates, R., Zidek, A., Potapenko, A., Bridgland, A., Meyer, C., Kohl, S. A. A., Ballard, A. J., Cowie, A., *et al.* (2021) Highly accurate protein structure prediction with AlphaFold. *Nature* **596**, 583–589
40. Qi, X., Liu, H., Thompson, B., McDonald, J., Zhang, C., and Li, X. (2019) Cryo-EM structure of oxysterol-bound human Smoothened coupled to a heterotrimeric Gi. *Nature* **571**, 279–283
41. Banasik, M., Komura, H., Shimoyama, M., and Ueda, K. (1992) Specific inhibitors of poly(ADP-ribose) synthetase and mono(ADP-ribosyl)transferase. *J. Biol. Chem.* **267**, 1569–1575
42. Jorgensen, R., Purdy, A. E., Fieldhouse, R. J., Kimber, M. S., Bartlett, D. H., and Merrill, A. R. (2008) Cholix toxin, a novel ADP-ribosylating factor from Vibrio cholerae. *J. Biol. Chem.* **283**, 10671–10678
43. Yates, S. P., Taylor, P. L., Jorgensen, R., Ferraris, D., Zhang, J., Andersen, G. R., and Merrill, A. R. (2005) Structure-function analysis of water-soluble inhibitors of the catalytic domain of exotoxin A from Pseudomonas aeruginosa. *Biochem. J.* **385**, 667–675
44. Lyons, B., Ravulapalli, R., Lanoue, J., Lugo, M. R., Dutta, D., Carlin, S., and Merrill, A. R. (2016) Scabin, a novel DNA-acting ADP-ribosyltransferase from Streptomyces scabies. *J. Biol. Chem.* **291**, 11198–11215
45. O'Neal, C. J., Jobling, M. G., Holmes, R. K., and Hol, W. G. (2005) Structural basis for the activation of cholera toxin by human ARF6-GTP. *Science* **309**, 1093–1096
46. Han, S., and Tainer, J. A. (2002) The ARTT motif and a unified structural understanding of substrate recognition in ADP-ribosylating bacterial

toxins and eukaryotic ADP-ribosyltransferases. *Int. J. Med. Microbiol.* **291**, 523–529
47. Brown, D. R., Keith, J. M., Sato, H., and Sato, Y. (1991) Construction and characterization of genetically inactivated pertussis toxin. *Dev. Biol. standardization* **73**, 63–73
48. Ausar, S. F., Zhu, S., Duprez, J., Cohen, M., Bertrand, T., Steier, V., Wilson, D. J., Li, S., Sheung, A., Brookes, R. H., Pedyczak, A., Rak, A., and Andrew James, D. (2020) Genetically detoxified pertussis toxin displays near identical structure to its wild-type and exhibits robust immunogenicity. *Commun. Biol.* **3**, 427
49. Locht, C., and Antoine, R. (1995) A proposed mechanism of ADP-ribosylation catalyzed by the pertussis toxin S1 subunit. *Biochimie* **77**, 333–340
50. Pizza, M., Covacci, A., Bartoloni, A., Perugini, M., Nencioni, L., De Magistris, M. T., Villa, L., Nucci, D., Manetti, R., Bugnoli, M., Giovannoni, F., Olivieri, R., Barbieri, J. T., Sato, H., and Rappuoli, R. (1989) Mutants of pertussis toxin suitable for vaccine development. *Science* **246**, 497–500
51. Kaslow, H. R., Schlotterbeck, J. D., Mar, V. L., and Burnette, W. N. (1989) Alkylation of cysteine 41, but not cysteine 200, decreases the ADP-ribosyltransferase activity of the S1 subunit of pertussis toxin. *J. Biol. Chem.* **264**, 6386–6390
52. Antoine, R., and Locht, C. (1994) The NAD-glycohydrolase activity of the pertussis toxin S1 subunit. Involvement of the catalytic HIS-35 residue. *J. Biol. Chem.* **269**, 6450–6457
53. Avigan, J., Murtagh, J. J., Jr., Stevens, L. A., Angus, C. W., Moss, J., and Vaughan, M. (1992) Pertussis toxin-catalyzed ADP-ribosylation of G(o) alpha with mutations at the carboxyl terminus. *Biochemistry* **31**, 7736–7740
54. Mateo, J., Lord, C. J., Serra, V., Tutt, A., Balmana, J., Castroviejo-Bermejo, M., Cruz, C., Oaknin, A., Kaye, S. B., and de Bono, J. S. (2019) A decade of clinical development of PARP inhibitors in perspective. *Ann. Oncol.* **30**, 1437–1447
55. Morrow, D. A., Brickman, C. M., Murphy, S. A., Baran, K., Krakover, R., Dauerman, H., Kumar, S., Slomowitz, N., Grip, L., McCabe, C. H., and Salzman, A. L. (2009) A randomized, placebo-controlled trial to evaluate the tolerability, safety, pharmacokinetics, and pharmacodynamics of a potent inhibitor of poly(ADP-ribose) polymerase (INO-1001) in patients with ST-elevation myocardial infarction undergoing primary percutaneous coronary intervention: Results of the TIMI 37 trial. *J. Thromb. Thrombolysis* **27**, 359–364
56. Purnell, M. R., and Whish, W. J. (1980) Novel inhibitors of poly(ADP-ribose) synthetase. *Biochem. J.* **185**, 775–777
57. Karlberg, T., Hammarstrom, M., Schutz, P., Svensson, L., and Schuler, H. (2010) Crystal structure of the catalytic domain of human PARP2 in complex with PARP inhibitor ABT-888. *Biochemistry* **49**, 1056–1058
58. Wahlberg, E., Karlberg, T., Kouznetsova, E., Markova, N., Macchiarulo, A., Thorsell, A. G., Pol, E., Frostell, A., Ekblad, T., Oncu, D., Kull, B., Robertson, G. M., Pellicciari, R., Schuler, H., and Weigelt, J. (2012) Family-wide chemical profiling and structural analysis of PARP and tankyrase inhibitors. *Nat. Biotechnol.* **30**, 283–288
59. Karlberg, T., Thorsell, A. G., Kallas, A., and Schuler, H. (2012) Crystal structure of human ADP-ribose transferase ARTD15/PARP16 reveals a novel putative regulatory domain. *J. Biol. Chem.* **287**, 24077–24081
60. Scheuring, J., Berti, P. J., and Schramm, V. L. (1998) Transition-state structure for the ADP-ribosylation of recombinant Gialpha1 subunits by pertussis toxin. *Biochemistry* **37**, 2748–2758
61. Scheuring, J., and Schramm, V. L. (1997) Kinetic isotope effect characterization of the transition state for oxidized nicotinamide adenine dinucleotide hydrolysis by pertussis toxin. *Biochemistry* **36**, 4526–4534
62. Scheuring, J., and Schramm, V. L. (1997) Pertussis toxin: Transition state analysis for ADP-ribosylation of G-protein peptide alphai3C20. *Biochemistry* **36**, 8215–8223
63. Ferro, A. M., and Oppenheimer, N. J. (1978) Structure of a poly (adenosine diphosphoribose) monomer: 2'-(5"-hosphoribosyl)-5'-adenosine monophosphate. *Proc. Natl. Acad. Sci. U. S. A.* **75**, 809–813
64. Moss, J., Garrison, S., Oppenheimer, N. J., and Richardson, S. H. (1979) NAD-dependent ADP-ribosylation of arginine and proteins by Escherichia coli heat-labile enterotoxin. *J. Biol. Chem.* **254**, 6270–6272
65. Oppenheimer, N. J. (1978) Structural determination and stereospecificity of the choleragen-catalyzed reaction of NAD+ with guanidines. *J. Biol. Chem.* **253**, 4907–4910
66. McCoy, A. J., Grosse-Kunstleve, R. W., Adams, P. D., Winn, M. D., Storoni, L. C., and Read, R. J. (2007) Phaser crystallographic software. *J. Appl. Crystallogr.* **40**, 658–674
67. Emsley, P., Lohkamp, B., Scott, W. G., and Cowtan, K. (2010) Features and development of Coot. *Acta Crystallogr. Sect. D, Biol. Crystallogr.* **66**, 486–501
68. Adams, P. D., Afonine, P. V., Bunkoczi, G., Chen, V. B., Davis, I. W., Echols, N., Headd, J. J., Hung, L. W., Kapral, G. J., Grosse-Kunstleve, R. W., McCoy, A. J., Moriarty, N. W., Oeffner, R., Read, R. J., Richardson, D. C., *et al.* (2010) Phenix: A comprehensive python-based system for macromolecular structure solution. *Acta Crystallogr. Sect. D, Biol. Crystallogr.* **66**, 213–221

Moona Sakari is a PhD student of Turku Cellular Microbiology Laboratory (https://twitter.com/ArtoPulliainen) at the Institute of Biomedicine, University of Turku, Turku, Finland. Her research is focused on gaining molecular level understanding on how bacterial effector proteins, especially those with ADP-ribosyltransferase activity, function during bacterial pathogen-host cell interaction. The results of her research could facilitate development of new and targeted therapeutic solutions to bacterial infections.